Physicochem. Probl. Miner. Process., 58(5), 2022, 151933

http://www.journalssystem.com/ppmp

Physicochemical Problems of Mineral Processing

ISSN 1643-1049

Diffuse-layer surface potentials of colemanites mined in Turkey

Dilek Senol-Arslan [1], Jaroslaw W. Drelich [2]

[1] Department of Nanotechnology Engineering, Abdullah Gul University, Kayseri 38380, Turkey

[2] Department of Materials Science and Engineering, Michigan Technological University, Houghton, MI 49931, USA

Corresponding author: dilekssenol@gmail.com (Dilek Senol-Arslan)

Abstract: Colemanite crystal specimens were handpicked at Kestelek, Emet (Hisarcik, Espey), Bigadic mines in Turkey for characterization of their composition and surface potential. X-ray diffraction analysis revealed no differences in mineralogical makeup of the crystals, but elemental analysis indicated differences in the type of trace (<0.1 wt%) elements. Zeta potential measurements showed small differences in zeta potential values, with isoelectric points (iep) varying from about pH = 9.6 to pH = 10.2. However, no correlation was found between iep and the type of trace elements. Additionally, atomic force microscopy (AFM) was employed to measure the colloidal interactions between a silicon nitride (Si3N4) cantilever tip and colemanite crystal surfaces in 1 wt% colemanite-saturated aqueous solutions at three different pHs (8.4, 9.4 and 11). The Derjaguin-Landau-Verwey-Overbeek theory (DLVO) was applied to examine the AFM tip interactions with colemanite surfaces in an aqueous solution of colemanite saturated solutions. The results revealed attractive forces at pH = 8.4 and 9.4 and repulsive forces at pH = 11, confirming the location of an isoelectric point for colemanite specimens somewhere between pH = 9.5 and pH = 10.1. Theoretical analysis of the force curves using the DLVO theory allowed for assessment of both surface charge density and surface potential for colemanite specimens used in this study.

Keywords: colemanite, surface potential, atomic force microscopy, boron, DLVO

1. Introduction

About 73% of world boron reserves are located in Turkey. Tincal and colemanite are the most abundant boron minerals, with colemanite constituting about 76% of Turkey's boron reserves. Colemanite ($Ca_2B_6O_{11}{\cdot}5H_2O$) is a hydrous calcium borate semi-soluble boron mineral. Colemanite deposits in Turkey are located in Kütahya – Emet, Balıkesir – Bigadiç and Bursa – Kestelek. The geological origins of the deposits, having varying mineralogical environments and natural ecosystems, affected the crystallographic and elemental characteristics of the boron minerals. Reactions between mineral surfaces and aqueous solutions, atmospheric gases, and biological organisms also contribute to rock formation and chemical weathering at the molecular level (Brown and Calas, 2012; Davis and Hayes, 1986) and have effects on colemanite. Therefore, the location of the colemanite mineral and the geological history of the deposit can influence the physical and chemical properties of colemanite. For example, both the type and valence of cation inclusions dictate the solubility of colemanite and mineral surface charge characteristics in an aqueous environment. There exists a considerable body of literature on the solubility of colemanite in various acids (Alkan and Doğan, 2004; Cetin et al., 2001; Saleem et al., 2011; Yeşilyurt et al., 2005).

After mining, colemanite ores are enriched in concentrator plants by physical processes such as crushing, grinding and dry classification to produce a concentrated product. Depending on the geochemical origins and mineralogical composition of the processed ore, different quantities and qualities of concentrate are produced. Bigadic colemanaite ore deposits are interbedded with clay, fine layered limestone, and tuffs (Helvaci, 1995) and contain elements such as Ca, Si, Mg, Al, Fe, S, Na, P and Mn (Koçak and Koç, 2012). Kestelek colemanite deposits are accompanied by calcite, tuff, marl, aragonite, smectite, illite, chlorite, heulandite, corrensite, limestone, rhyolite, and quartz. Ca Si, Mg, Al,

DOI: 10.37190/ppmp/151933

Fe, K, Na, P, and Ti are the typical elements found in Kestelek colemanite ore (Koç et al., 2017). Clays generally surround Emet colemanite (Espey and Hisarcik) nodules as a film (Koçak and Koç, 2018). This formation contains quartz, zeolites, tuffs, illite-smectite, calcite, feldspar, clinoptilolite, realgar, orpiment, celestite and native sulfur (Çolak et al., 2000; Helvaci, 1977). As, Se, Cs, Li, Sr and Sb are typically associated with the Emet deposits (Koçak and Koç, 2018; Özkul et al., 2017). In Turkey, colemanite deposits were formed in lacustrine environments where volcanic activities started from the early Tertiary and continued until the Quaternary (Helvaci and Alonso, 2000). The above-mentioned impurities that pass into the solution significantly affect the product quality and separation methods.

Understanding of the bulk and surface characteristics of colemanite is of fundamental importance in processing of the ores and in industrial uses like manufacturing of heat resistant glass and advanced technological materials. Colemanite mineral surface characteristics have not been sufficiently studied, especially for colemanite of different origins.

In this study, the colemanite specimens were handpicked at Kestelek, Emet (Hisarcik, Espey), and Bigadic. The natural boron mineral crystals are of different origins, having a specific elemental composition and crystal structure. As is known, during regional metamorphism mineral content and texture are changed due to the changes in the physical (temperature, pressure) and chemical (recrystallization) environment of the rock (Helvaci, 2015; Helvaci and Alonso, 2000). Although each of these specimens were surrounded by different gangue minerals they retain their own characteristics. For this reason, it was aimed to investigate the differences in surface potentials of colemanite crystals obtained from four different regions.

2. Materials and methods

2.1. Materials

The colemanite minerals were collected in the form of lump-sized crystals from Bigadic, Kestelek, and Emet (Espey and Hisarcik) deposits of Turkey from Eti Mine Works (Fig. 1). All samples were cleaved 15×15×5 mm and polished with 0.06 μm alumina powder, then rinsed with DI water for the AFM measurements. The chemicals used in this study include sodium hydroxide (NaOH, Merck KGaA) and hydrochloric acid (HCl, Merck KGaA). A Milli-Q water system (Millipore) ensured high-purity water (18.2 MΩ.cm).

Fig. 1. Photographs of colemanite crystals

2.2. Methods

2.2.1. Colemanite crystals characterization

Crystallographic structure of the colemanite samples was determined using a Bruker D8 Discover diffractometer equipped with a Cu Target X-ray tube operating at 40 kV and 30 mA. The samples used for XRD analysis were prepared by grinding handpicked crystals down to –38μm.

The elemental composition of the colemanite samples was analyzed using a Perkin Elmer ELAN DRC-e 6000 ICP/MS (inductively coupled mass spectrometer). The –38 μm colemanite powders were ionized in a plasma (ICP) and then sent to mass spectroscopy (MS) where they were recorded by their mass/charge (m/z) ratios.

The colemanite sample surfaces were imaged with a GeminiSEM 300 scanning electron microscope using 10 kV accelerated voltage. All of the SEM measurements were performed on the colemanite crystals which were used in AFM force measurements.

For topographical imaging of individual colemanite crystals and determination of their surface roughness, a Nanoscope III Dimension 3000 atomic force microscope (Digital Instruments, Santa

Barbara, CA, USA) was employed in a tapping mode operation. Budget Sensors Tap300Al cantilevers made of silicon with an aluminum reflex coating, and an estimated tip radius of 10 nm were used in this study.

2.2.2. Zeta potential measurements

Zeta potential measurements of the colemanite samples were performed by the electrophoresis technique using ZetaPlus (Brookhaven Instrument Corporation, USA). It automatically calculates the electrophoretic mobility of colemanite particles and converts it to the zeta potential using the Smoluchowski equation (Eq.1) (Smoluchowski 1921). The sample used for zeta potential determination was prepared by grinding the colemanite crystals down to –10 μm. The samples were prepared at solids concentration of 1wt.%. The pH was adjusted by 0.1 M HCl and NaOH. Each data point represents an average of about 20 measurements. All of the measurements were carried out at room temperature.

$$\zeta=\frac{4\pi\eta}{\varepsilon}xU \tag{1}$$

where, ζ : zeta potential, ε:dielectric constant, η: viscosity, U: electrophoretic mobility

2.2.3. Force measurements

Aqueous suspensions of saturated solutions were made with –38 μm colemanite particles at solids concentration of 1wt.%. The pH was adjusted by 0.1 M HCl and NaOH. The colloidal forces were measured between silicon nitride and flat colemanite crystal substrates in saturated colemanite suspensions as a function of three different pHs (8.4, 9.4, and 11). Contact-mode silicon nitride (Si_3N_4) AFM cantilevers of a V-frame shape (Bruker AFM Probes, Camarillo, CA), having pyramidal-shaped tips with an apex curvature radius of ca. 10 nm and a spring constant of ca. 0.12 N/m were used in this study. An accurate value of the spring constant was determined using the thermal tune method available in the AFM software package. The apex curvature radius of about 10 nm for each tip was confirmed by imaging the tips under the field emission scanning electron microscope (S-4700 FE-SEM, Hitachi High Technologies America, Schaumburg, IL).

The force curves were recorded at each pH and for each specimen, and only representative curves are reported here. All of the force curves were analysed with SPIP software (Image Metrology, Lyngby, Denmark), which translates the cantilever deflection-piezo extension/retraction data to force-separation curves including estimation of a zero-separation distance; the additional processing of the force-distance curve included baseline correction and hysteresis correction.

The use of saturated solutions caused nucleation and growth of nano-sized crystals on the surface of the cantilever that scattered a laser beam and reduced the signal on the photodetector, eliminating the possibility of precise and multiple recording of cantilever deflection. For that reason, the recording of forces was limited to the first 10-20 runs and in solutions of three different pHs.

2.2.4. Determination of Hamaker constant

Advancing contact angles (θ) were measured for apolar liquid diiodomethane having a surface tension of γ_L=50.8 mN/m, on the surfaces of colemanite crystals at room temperature (20-22°C). The measurements were performed with the sessile drop method, using a Krüss G10 contact angle goniometer according to protocol described previously (Drelich, 2013).

The surface tension of diiodomethane and its components are shown in Table 1. These surface tension components yield to the equation:

$$\gamma_{L\,(1+\cos\theta)} = 2\left[\sqrt{\gamma_S^{LW}}\gamma_L^{LW} + \sqrt{\gamma_S^{+}\gamma_L^{-}} + \sqrt{\gamma_S^{-}\gamma_L^{+}}\right] \tag{2}$$

By measuring contact angle for apolar diidomethane, the Lifshits-van der Waals surface tension of colemanite (γ_S^{LW}) was calculated using the following equation:

$$\gamma_S^{LW} = \frac{\gamma_L\,(1+\cos\theta)^2}{4} \tag{3}$$

After obtaining γ_S^{LW} , the average Hamaker constant was calculated by:

$$A = 1.44x10^{-18}\gamma_S^{LW} \tag{4}$$

The total constant Aii, controlling the interaction between the two bodies at short distances. For two materials 1 and 2, immersed in medium 3, the combining rules were described by:

$$A_{132} = \left(\sqrt{A_{11}} - \sqrt{A_{33}}\right)\left(\sqrt{A_{22}} - \sqrt{A_{33}}\right) \quad (5)$$

Table 1. Surface tension components of contact angle probe liquid (C.J.van Oss 1986; Oss 1994). γ^{LW} is the Lifshitz-van der Waals surface tension, where subscripts L and S refer to solid and liquid, γ- and γ+ are the Lewis acidic (electron acceptor) and basic (electron donor).

Liquid	γ_L	γ_L^{LW}	γ^-	γ^+
Diiodomethane	50.8	50.8	0	0

2.2.5. Theoretical model for surface forces

2.2.5.1. DLVO Model for Force-Distance Curves

Geometry of the AFM tip (Si_3N_4)-substrate (colemanite) system in colloidal force measurements and the parameters used in the modeling and the equations on DLVO forces, a combination of van der Waals and electrostatic forces, are well described in the literature (Drelich, 2007) and will not be repeated here. The van der Waals forces (F^{vdW}) were modeled according to the following Eq. 6:

$$F^{vdW} = \frac{A}{6}\left[\frac{(R+D)-2L_1}{L_1^2} - \frac{R-D}{D^2}\right] - \frac{A}{3\,tan^2\alpha}\left[\frac{1.0}{L_1} + \frac{R\,\sin\alpha - D - R\,(1-\cos\alpha)}{L_1^2}\right] \quad (6)$$

The equation describing the electrostatic force (Fedl, constant surface-charge density case) is as follows:

$$F^{edl} = \frac{4\pi}{\varepsilon_0\,\varepsilon\kappa^2}\,\alpha_T\alpha_S(a_0\,e^{-\kappa D} - a_1\,e^{-\kappa L_1}) + \frac{2\pi}{\varepsilon_0\varepsilon\,\kappa^2}\,(\sigma_T^2 + \sigma_S^2) \quad (7)$$

$$(a_2 e^{-2\,\kappa D} - a_3\,e^{-2\kappa\,L_1}) + \frac{4\pi}{\varepsilon_0\,\varepsilon\kappa\,\tan\alpha}\left[b_1\sigma_T\sigma_S e^{-\kappa L_1} + b_2\,\frac{(\sigma_T^2+\sigma_S^2)}{2}\,e^{-2\kappa L_1}\right] \quad (8)$$

where:

L_1=D+R(1-cos α), a_0= κ R-1, a_1 = κR cos α -1, a_2= a_0+0.5, and a_3= a_1 +0.5

$$b_1 = \left[R\sin\alpha - \frac{D+R(1-\cos\alpha)}{\tan\alpha}\right] + \frac{1}{\tan\alpha}\left[\left(L_1\,\frac{1}{\kappa}\right)\right] \quad (9)$$

$$b_2 = \left[R\sin - \frac{D+R(1-\cos\alpha)}{\tan\alpha}\right] + \frac{1}{\tan\alpha}\left[\left(L_1\,\frac{1}{2\kappa}\right)\right] \quad (10)$$

α and β are the geometrical angles for the spherical cap at the tip end and conical tip with α +β=90°, A is the Hamaker constant, D is the distance from the end of the tip to the substrate, L_1 is the distance between a differential surface section of the tip and the substrate, r is the radius of the circle of the tip at a given vertical position, R is the radius of the spherical cap at the tip end, ε is the dielectric constant of the solution in this system, ε_0 is the permittivity of vacuum, 1/κ is the Debye length, σ is the surface-charge density, and subscripts S and T refer to the substrate and tip, respectively (Drelich, 2007).

The total DLVO force for the system is given by adding the electrostatic force and the van der Waals force:

$$F = F^{vdW} + F^{edl} \quad (11)$$

2.2.5.2. The case of constant surface charge density

The electrostatic force between the tip and substrate under the case of constant surface charge density can be obtained from Eq. 10.

$$F_{TS}^S = \frac{4\pi}{\varepsilon_0\varepsilon\kappa^2\tan\alpha}\sigma_T\sigma_S(a_0 e^{-\kappa L_1} - a_1 e^{-\kappa L_1}) + \frac{2\pi}{\varepsilon_0\,\varepsilon\,\kappa^2}(\sigma_T^2 - \sigma_S^2)(a_2 e^{-2\kappa D} - a_3 e^{-2\kappa L_1}) \quad (12)$$

while in the conical region, it is changed to:

$$F_{TS}^C = \frac{4\pi}{\varepsilon_0\,\varepsilon_\kappa\tan\alpha}\left[b_1\sigma_T\sigma_S e^{-\kappa L_1} + b_2\,\frac{(\sigma_T^2+\sigma_S^2)}{2}\,e^{-\kappa L_1}\right] \quad (13)$$

2.2.5.3. Colemanite surface potential

The surface potential of colemanite was calculated based on fitted surface charge density values using the Graham equation (Israelachvili, 1992). This equation is introduced to obtain the relationship between the concentration of ions at an isolated surface and the surface charge density (σ).

$$c_0 - c_\infty = \frac{\sigma^2}{2\varepsilon\varepsilon_0 kT} \tag{14}$$

where c_0 is the ionic concentration on the surface, and c_∞ is the ionic concentration in the bulk (at x=∞) where Φ∞=0.

$$c_0 = c_\infty exp\left(-\frac{z_i e\,\Phi}{kT}\right) \tag{15}$$

where the ionic concentration in the bulk solution is given by:

$$c_\infty = \frac{\kappa\,\varepsilon\,\varepsilon_0 kT}{e^2 z^2} \tag{16}$$

3. Results and discussion

3.1. Colemanite crystals characterization

The XRD patterns of colemanite samples are shown in Fig.2. The patterns appear nearly identical, suggesting the absence of mineralogical impurities. As no other phase was detected, we can reasonably conclude that all four colemanite crystal powders are phase-pure $Ca_2B_6O_{11}.5H_2O$. The degree of crystallinity was automatically calculated from the XRD patterns as 93.3%, 92.5%, 92.3%, and 93%, for Bigadic, Espey, Hisarcik and Kestelek colemanite, respectively. Because of the crystal purity, all samples have high peak intensity. We focused on 20 major diffraction peaks. ICDD indexing of these peaks are referred to PDF 33-0267.

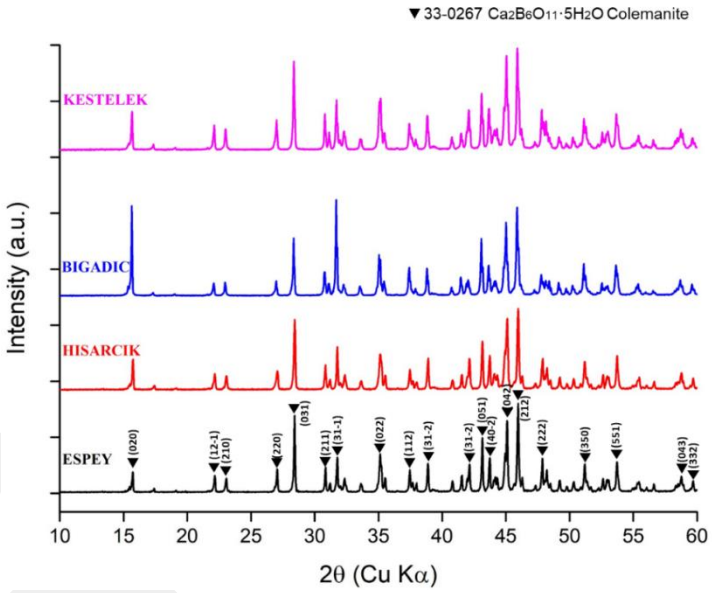

Fig. 2. XRD patterns of Espey, Hisarcik, Bigadic and Kestelek colemanite samples

3.2. Elemental composition

It is known that elements such as As, S, Li, Sr, Sb, Pb, and Mn are commonly found in different amounts in rich boron deposits in Western Anatolia (Kocak, 2020; Ok and Akay, 2016). It has been stated that the common source of the formation of these elements in the Neogene basins is the thermal and hydrothermal resources associated with volcanic activities (Helvaci, 2015).

According to the ICP/MS analysis (Table 2) the colemanite samples have high amounts of boron and calcium (B, Ca) elements and only trace amounts of other elements. All crystals contained traces of Cu, Sr, Mo, and U. Na was detected in Bigadic, Kestelek, and Hisarcik, Fe and Zn in Bigadic and Espey. Kestelek and Espey additionally contained Ag and Pb, and Sn and W, respectively.

3.3. Zeta potential measurements

Colemanite is a semi-soluble mineral and exhibits a spectrum of chemical compositions with different cation inclusions. When colemanite dissolves in water, it releases a number of ionic species. These ions

adsorb back at the mineral/liquid interface. The dissolution process for colemanite occurs in a system open to the atmosphere producing 5.10^{-3}M solution (2.1 g of colemanite/L) (Celik and Yasar, 1995; Ozdemir and Celik, 2010).

$$2CaO \cdot 3B_2O_3 \cdot 5H_2O + 4CO_2 + 6H_2O \leftrightarrow 2Ca^{2+} + 6H_3BO_3 + 4HCO_3^-$$

The result of zeta potential measurement of colemanite samples are shown in Figure 3.

Table 2. Quantitative ICP / MS analysis of colemanite crystals in four different regions

Region	Trace elements (< 0.1 wt%)	High
Bigadic	Na, Fe, Cu, Zn, Sr, Mo, U	B, Ca
Kestelek	Na, Cu, Sr, Mo, Ag, Pb, U	B, Ca
Espey	Fe, Cu, Zn, Sr, Mo, Sn, W, U	B, Ca
Hisarcik	Na, Cu, Sr, Mo, U	B, Ca

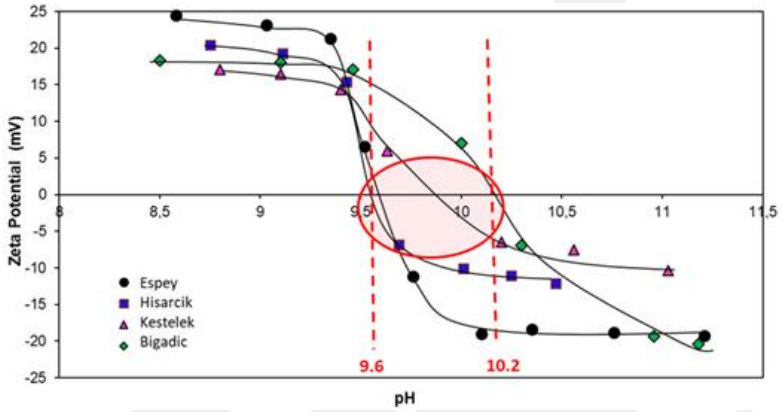

Fig. 3. Zeta potential values of different pHs for 4 different originated colemanites

The experimental data on zeta potential clearly show that the values of the different originated colemanite crystals depend on pH (Fig.3). The isoelectric point (iep) value of colemanite changes between pH=9.6 and pH=10.2. Below the iep, the colemanite is positively charged and negatively charged above it. The system as a whole must be electrically neutral. Thus, there should be an equivalent amount of counter ions (charge opposite to the surface) in the interfacial zone. Potential determining ions (pdi) for colemanite are found to be lattice cations, i.e. Ca^{+2} and $B_4O_7^{2-}$ (borate), H^+ and OH^- ions which control ratio of HCO_3^-/CO_3^{2-} (Rousseau, 1987; Yarar, 1985).

The iep values for colemanite samples that originated from Bigadic and Espey are close to the literature values, as presented in Table 3.

Table 3. Isoelectric point (iep) of colemanite reported in the literature

Colemanite (Origin)	Isoelectric point (iep)	References
Bigadic	10.5	(Celik and Yasar, 1995)
Bigadic	10.5	(Celik et al., 2002)
Bigadic	10.2	(Sahinkaya and Ozkan, 2011)
Espey	10.2	(Ucar and Yargan, 2009)

Differences in the zeta potentials (electrokinetic potentials) of the colemanite samples were investigated by dissolution-precipitation processes at the mineral-solution interfaces. It has been observed that this process depends on the solubility product and concentration of pdi, particularly Ca^{2+} ions, that dominates in solution. It is interesting to notice that no correlation was found between zeta potential values and the presence of trace elements in the structure of colemanite crystals (see Table 1). However, both samples from Espey and Hisarcik showed identical iep, ~pH = 9.6. This suggests that the differences in zeta potential might be related to different geochemical origins of the colemanite. The

Espey and Hisarcik samples are from two different locations, although they represent the same mineral deposit.

3.4. Contact angles and Hamaker constant

Fig. 4 shows diiodomethane drops resting on flat, horizontal colemanite surfaces, and measured contact angle values. The Hamaker constant of each mineral was calculated from the contact angle values, and the calculated values are presented in Table 3. The Hamaker constant varied from about 4.9×10^{-19}J for Hisarcik to 6.3×10^{-19}J for Bigadic.

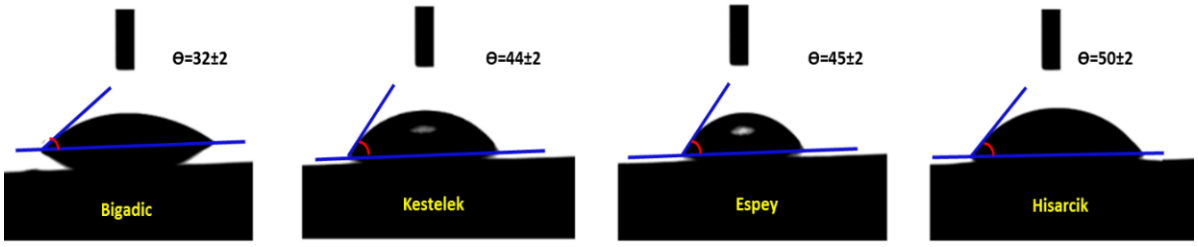

Fig. 4. Illustration of contact angles formed by sessile liquid drops on 4 different originated colemanite minerals smooth surface

Table 4. Hamaker constants of different originated colemanite crystals

Surface	Contact Angle (deg.)	Hamaker constant, J
Bigadic	32 ± 3	$6.3 \pm 0.2\text{x}10^{-19}$
Hisarcik	50 ± 2	$4.9 \pm 0.2\text{x}10^{-19}$
Espey	45 ± 2	$5.3 \pm 0.2\text{x}10^{-19}$
Kestelek	44 ± 2	$5.4 \pm 0.2\text{x}10^{-19}$

Table 5 presents all Hamaker constants for all three phases involved in interactions during AFM measurements and discussed in the next section. The Hamaker constant for water and silicon nitride were taken from previous reports. More accurate calculations could involve the Hamaker constant for a colemanite-saturated water solution but this correction could not make any significant impact on this overall crude approach in calculating Hamaker constant for the three-phase system.

Table 5. The Hamaker constant for phases and the silicon nitride-water-colemanite system

Mineral	A_{11} (Si_3N_4) (J)	A_{22}(Colemanite) (J)	A_{33}(Water) (J)	A(colemanite-water-Si_3N_4) (J)
Kestelek	1.6×10^{-19}	5.4×10^{-19}	3.7×10^{-20}	1.1×10^{-19}
Hisarcik	1.6×10^{-19}	4.9×10^{-19}	3.7×10^{-20}	1.1×10^{-19}
Espey	1.6×10^{-19}	5.3×10^{-19}	3.7×10^{-20}	1.1×10^{-19}
Bigadic	1.6×10^{-19}	6.3×10^{-19}	3.7×10^{-20}	1.2×10^{-19}

3.5. Colloidal forces and surface charges

3.5.1. Surface quality

Polished specimens used in the AFM colloidal force measurements were smooth at a nanoscale. Figures 5 and 6 show examples of both AFM and SEM images, respectively. Although specimens had polishing scratches and defects, as reflected by the SEM images, these regions were easy avoided when the AFM cantilever tip was launched into contact with the mineral surface. Typical arithmetic and geometrical roughness of the colemanite surface used in colloidal force measurements varied from less than 2 nm to 3-4 nm, and no significant differences in roughness were found between the four colemanite minerals.

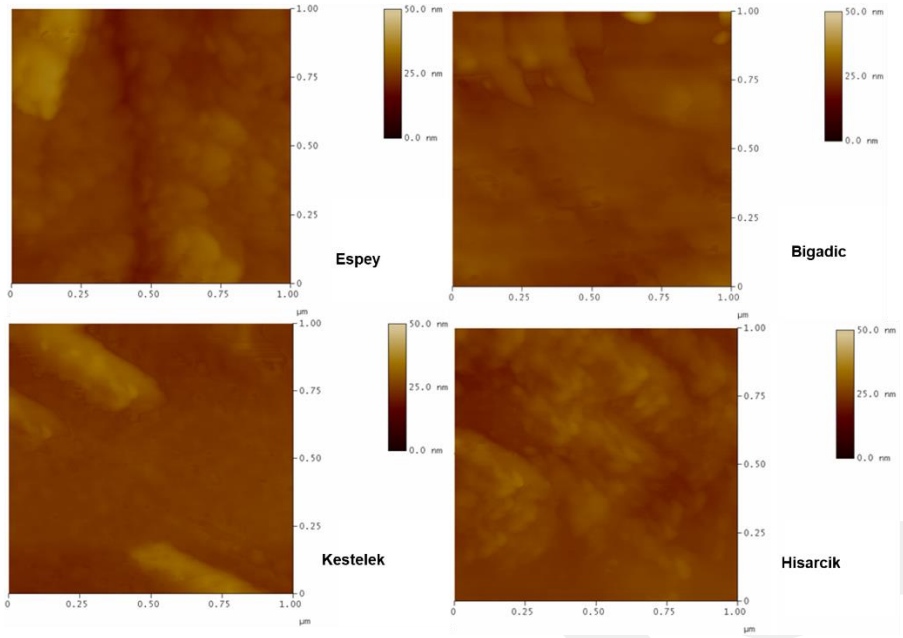

Fig. 5. AFM images of colemanite crystals used in colloidal force measurements

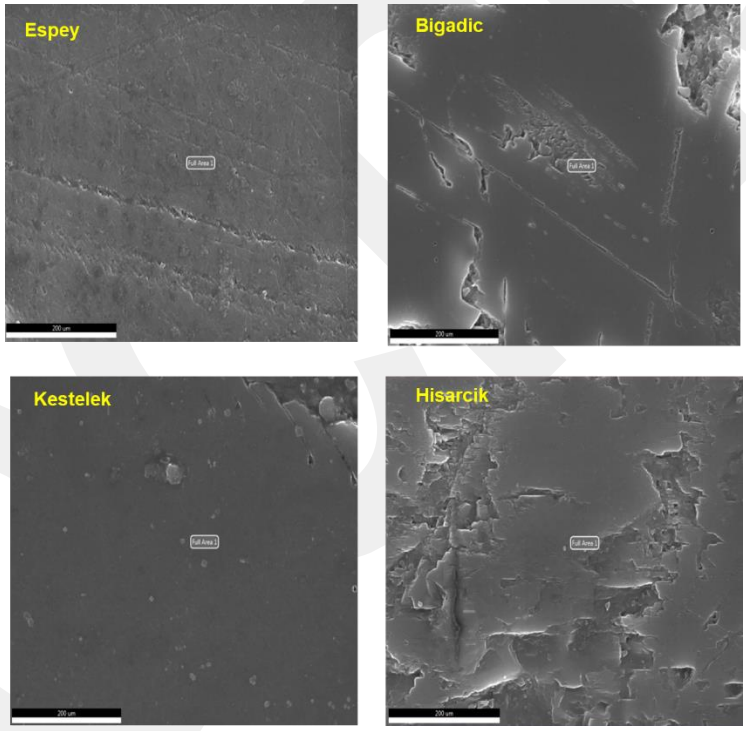

Fig. 6. SEM images of colemanite crystals used in colloidal force measurements. Scale bars at the left bottoms of images represent 200 μm

3.5.2. Force Curves

In this study, the force measurements where limited to three pHs: 8.4, 9.4, and 11. Measurements of colloidal forces in colemanite-saturated solution was obscured by the nucleation and formation of crystals on the surface of the AFM cantilever. These crystals scattered the laser beam and affected readings of cantilever deflection.

As has been previously reported in the literature, the Si_3N_4 AFM tip is negatively charged in pH ranges from 4−11.4 (Yin et al.,2008). Therefore, the sign of the mineral surface charge controls the attractive or repulsive interaction force between the cantilever tip and the mineral surface. A repulsive

force was observed when the mineral surface charge was negative, while an attractive force was observed when it was positive. For each of the colemanite samples, examples of representative force curves together with theoretical fittings are shown in Figure 6. The repulsive force dominated the interactions at pH 11 for each of the colemanite crystals. At pH 8.4 and pH 9.4, the force became more and more attractive. This variation of the force with different pH can be explained with the electrostatic and van der Waals forces. The vdW attraction is independent of pH, but electrostatic force changes due to changes in the surface charge of colemanite. The attractive electrostatic force is the result of positively charged colemanite and negatively charged silicon nitride at pH 8.4 and pH 9.4. At pH 11 only repulsive forces were recorded because both colemanite and silicon nitride are negatively charged.

3.5.3. Theoretical Fits

In all measurements, the experimental data were compared with theoretical calculations. Both the van der Waals forces (vdW) and the electrical double layer forces were described by the DLVO theory (Drelich J., 2005). Theoretical force-separation curves were plotted that fit to experimental curves using surface charge density of the substrate as an adjustable parameter. As shown in Fig.7, the experimental force curves are in good agreement with theoretical fitting curves.

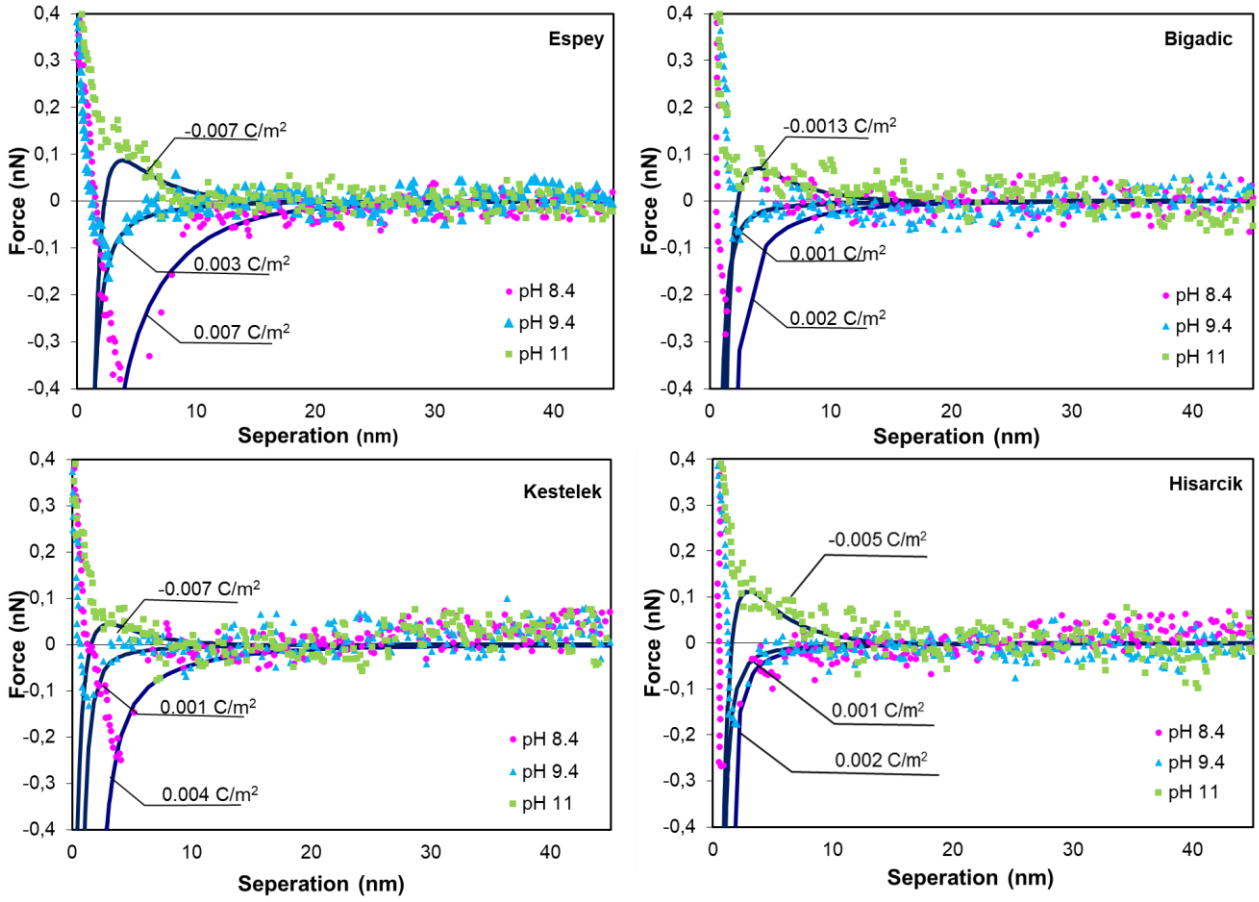

Fig. 7. Force versus separation curves obtained for a Si_3N_4 tip on 4 different originated colemanite crystals in colemanite saturated solutions at different pH (8.4, 9.4 and 11). Solid lines represent results of theoretical modeling. Radius of the tip end, R=10 nm, Hamaker constant $A=3.10^{-19}$J, Debye length, κ^{-1} = 4.3 nm, surface charge densities are shown on graph for each crystal. The Debye length is an estimated value based on expected concentrations of colemanite ions in aqueous saturated solutions

The surface charge density as a function of pH for four different originated colemanite mineral calculated from AFM force curves. Using the Graham equation, the surface potential of these were also calculated and plotted (Fig. 8). The results indicate that the surface of colemanite was positively charged at pH 8.4 and pH 9.4 and negatively charged at pH 11. Figure 8 shows the comparison between the zeta

potential values and surface potential values as determined with the AFM technique at three different pHs for each crystal. In spite of challenges associated with a high ionic strength of aqueous solution that was saturated with semi-soluble colemanite mineral, the results of iep are remarkably close to each other.

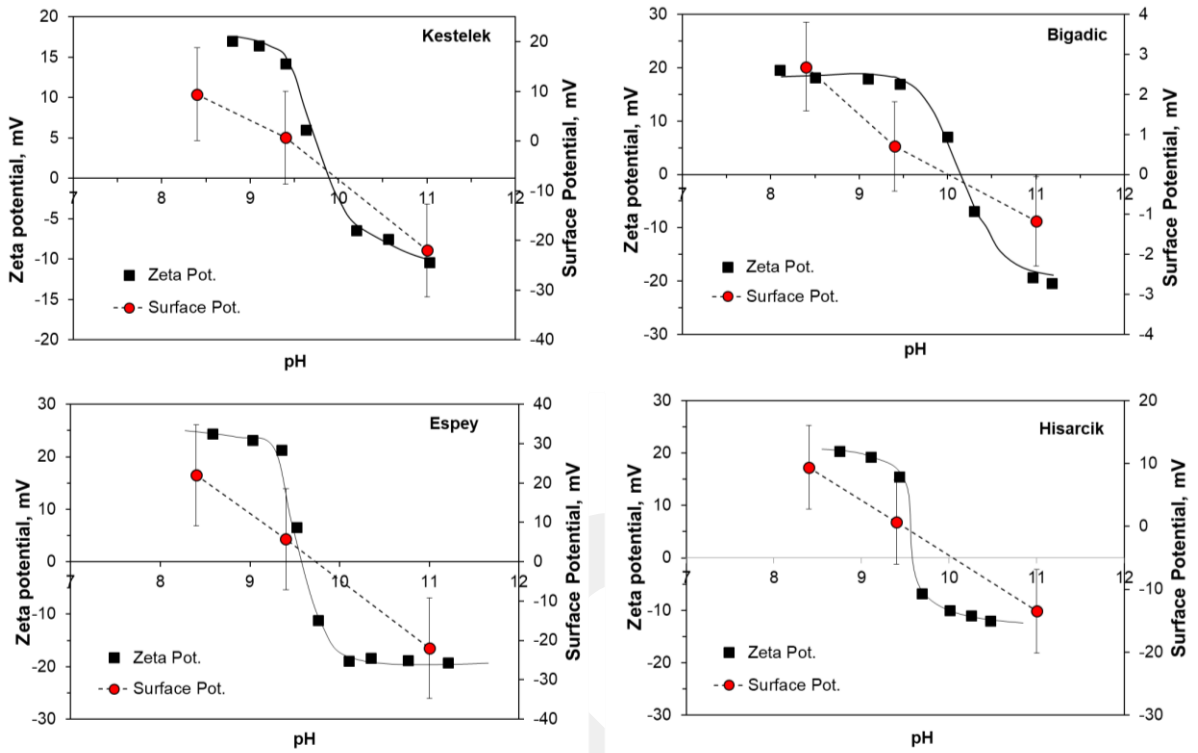

Fig. 8. A comparison of experimental zeta potential with calculated surface potential for four colemanite minerals

4. Conclusions

The colemanite crystal specimens from Kestelek, Emet (Hisarcik, Espey), and Bigadic mines appear to have identical mineralogical composition. However, the crystals contained different trace elements. In spite of similarities in mineralogical composition, the specimen surfaces exhibited a variation in electrophoretic mobility and calculated zeta potential values. The isoelectric point of colemanite increased from about pH = 9.6 for both Epsey and Hisarcik to pH = 9.8 for Kestelek and to pH = 10.2 for Bigadic. No correlation between iep and type of trace elements was found. However, similarity in iep for samples from Epsey and Hisarcik, originating from the same mineral deposit, suggest that differences in surface charge characteristics might be related to the geological origin of deposition.

Due to the high ionic strength of colemanite-saturated solutions, the experimental colloidal interactions measured with atomic force microscopy were limited to three pHs. The theoretical analysis of AFM experimental force curves based on the DLVO model confirmed negative surface potentials at pH = 8.4 and pH = 9.4 and positive surface potentials at pH = 11 of colemanite crystals, and location of isoelectric point in between pH = 9.5 and pH = 10.2.

Acknowledgments

The authors would like to thank Professor Orhan Ozdemir for helpful guidance in zeta potential measurements. This work was supported by The Scientific and Technological Research Council of Turkey (TUBITAK, Project no: 1059B141400362) and Scientific Research Projects Coordination Unit of Istanbul University (Project no: 42265).

This manuscript is dedicated to honour student mentor and our dear colleague Professor Mehmet Sabri Celik.

References

ALKAN M., DOĞAN M 2004. *Dissolution kinetics of colemanite in oxalic acid solutions.* Chemical Engineering and Processing, Process Intensification 43, 867-872.

BROWN, Jr GE., CALAS G., *2012. Mineral-aqueous solution interfaces and their impact on the environment.* Geochemical Perspectives 1, 483-484.

CELIK, M., HANCER M., MILLER J., 2002. *Flotation chemistry of boron minerals.* Journal of colloid and interface science 256, 121-131.

CELIK, M., YASAR E., 1995. *Electrokinetic properties of some hydrated boron minerals.* Journal of colloid and interface science 173, 181-185.

CETIN, E., EROGLU, İ., OZKAR, S., 2001. *Kinetics of gypsum formation and growth during the dissolution of colemanite in sulfuric acid.* Journal of Crystal Growth 231, 559-567.

COLAK, M., HELVACI C., MAGGETTİ., M., 2000. *Saponite from the Emet colemanite mines,* Kütahya, Turkey Clays and Clay Minerals 48, 409-423.

DAVIS, JA., HAYES KF., 1986. *Geochemical processes at mineral surfaces, an overview*

DRELICH, J., LONG, J., *and Yeung, A.,* 2007. *Determining Surface Potential of the Bitumen-Water Interface at Nanoscale Resolution using Atomic Force Microscopy.* The Canadian Journal of Chemical Engineering 85.

DRELICH, J. KLM 2005. *Atomic Force Microscopy in Adhesion Studies.* CRC Press, Taylor & Francis Group.

DRELICH, J., *Guidelines to measurements of reproducible contact angles using a sessile-drop technique*. Surface innovations, 2013. 1(4), 248-254.

HELVACI, C., 1977. *Geology, mineralogy and geochemistry of the borate deposits and associated rocks at the Emet Valley,* Turkey. University of Nottingham

HELVACI, C., 1995. *Stratigraphy, mineralogy, and genesis of the Bigadiç borate deposits, Western Turkey Economic Geology* 90, 1237-1260.

HELVACI, C., 2015. *Geological features of Neogene basins hosting borate deposits, an overview of deposits and future forecast,* Turkey Bulletin of the Mineral Research and Exploration 151, 169-215.

HELVACI, C., ALONSO, RN., 2000. *Borate deposits of Turkey and Argentina; a summary and geological comparison* Turkish Journal of Earth Sciences 9, 1-27.

ISRAELACHVILI, J., 1992. *Intermolecular and Surface Forces.* Vol 2nd ed. Academic Press Inc., San Diego

KOCAK, I., 2020 *Geochemistry of the Igdekoy-Doganlar Na-Ca borate deposit, Emet Province western Anatolia, Turkey.* Geological Quarterly 64, 807-817; doi, 810.7306/gq. 1555.

KOC, S., KAVRAZLI, O., KOCAK, I., 2017. *Geochemistry of Kestelek colemanite deposit, Bursa, Turkey.* Journal of Earth Science 28, 63-77.

KOCAK, I., KOC, S., 2012. *Major and trace element geochemistry of the Bigadiç Borate deposit, Balikesir, Turkiye.* Geochemistry International 50, 926-951.

KOCAK, I., KOC, S., 2018. *Geochemical characteristics of The Emet (Espey-Hisarcik) borate deposits.,* Kütahya, Turkey Journal *of African Earth Sciences* 142, 52-63.

OK, SS., AKAY, A., 2016. *The Effects of Boron Mining on Boron Content of Soil-Sediment and Plants.* International Journal of Innovative Research in Engineering & Management (IJIREM) ISSN, 2350-0557, Volume-3, Issue-5

OZDEMIR, O., CELİK, MS., 2010. *Surface properties and flotation characteristics of boron minerals.* The Open Mineral Processing Journal 3.

OSS CJv., 1994. *Interfacial Forces in Aqueous Media Marcel Dekker*, New York.

OZKUL, C., CİFTCİ, E., TOKEL, S., SAVAS, M., 2017. *Boron as an exploration tool for terrestrial borate deposits, A soil geochemical study in Neogene Emet-Hisarcık basin where the world largest borate deposits occur Kütahya-western Turkey.* Journal of Geochemical Exploration 173, 31-51.

ROUSSEAU, RW., 1987. *Handbook of Separation Process Technology. Wiley,*

SAHINKAYA, HU., OZKAN, A., 2011. *Investigation of shear flocculation behaviors of colemanite with some anionic surfactants and inorganic salts.* Separation and Purification Technology 80, 131-139.

SALEEM, M., KHANIFY, Y., ISHAK, YF., SAMSURI, A., 2011. *Solubility and leaching of boron from borax and colemanite in flooded acidic soils.* Communications in soil science and plant analysis 42, 293-300.

SMOLUCHOWSKI M., 1921. *Handbuch der Elektrizität und des Magnetismus Band II,* Barth-Verlag, Leipzig, 366-427.

UCAR, A., YARGAN, M., 2009. *Selective separation of boron values from the tailing of a colemanite processing plant.* Separation and Purification Technology 68, 1-8.